

1 **Altitude Registration of Limb-Scattered Radiation**

2
3
4
5
6
7
8
9
10
11
12
13
14
15
16
17
18
19
20
21
22
23
24
25
26
27
28
29
30
31

Leslie Moy¹, P.K. Bhartia², Glen Jaross², Robert Loughman³, Natalya Kramarova¹, Zhong Chen¹, Ghassan Taha⁴, Grace Chen¹, and Philippe Xu⁵

[1] Science Systems and Applications, Inc. (SSAI), 10210 Greenbelt Road, Suite 600, Lanham, Maryland 20706 USA

[2] NASA Goddard Space Flight Center, Greenbelt, Maryland, USA

[3] Hampton University, Hampton, Virginia USA

[4] GESTAR, Columbia, MD USA

[5] Science Applications International Corporation (SAIC), Lanham, MD

Correspondence to: Leslie Moy (leslie.moy@ssaihq.com)

32 **Abstract**

33

34 One of the largest constraints to the retrieval of accurate ozone profiles from UV backscatter
35 limb sounding sensors is altitude registration. Two methods, the Rayleigh Scattering Attitude
36 Sensing (RSAS) and Absolute Radiance Residual Method (ARRM), have been developed to
37 determine the altitude registration to the accuracy necessary for long-term ozone monitoring. The
38 methods compare model calculations of radiances to measured radiances, and are independent of
39 onboard tracking devices. RSAS determines absolute altitude errors, but because the method is
40 susceptible to aerosol interference, it is limited to latitudes and time periods with minimal
41 aerosols. ARRM can be applied across all seasons and altitudes. However, it is only appropriate
42 for relative altitude error estimates. The application of these methods to Ozone Mapping and
43 Profiler Suite (OMPS) Limb Profiler (LP) measurements showed that, at launch, the OMPS LP
44 instrument had a 1-2 km altitude registration error, resulting in a 50% error in the derived ozone
45 density at some altitudes. Though some of the error has been attributed to thermal shifts in the
46 focal plane of the instrument, most of it appears to be due to misalignment of the spacecraft star
47 trackers or the OMPS LP focal plane with respect to the spacecraft axes. In addition, there are
48 ± 200 m seasonally varying errors that could either be due to errors in the spacecraft pointing
49 information or in the geopotential height (GPH) data that we use in our analysis.

50

51

52

53

54

55

56

57

58

59

60 **Keywords: altitude registration, OMPS Limb Profiler, RSAS, ARRM, ozone profile,**
61 **backscattered ultraviolet**

62

63 **1 Introduction**

64 Instruments that measure the solar radiation scattered by the earth's atmosphere in the limb
65 direction provide a low cost way of measuring stratospheric ozone and aerosols from satellites.
66 The technique provides daily full coverage of the sunlit earth from commonly used polar sun-
67 synchronous satellites. To meet the science requirements for monitoring ozone requires the
68 altitude registration of the radiances to be accurate to within ~ 100 m. For a sensor orbiting at 800
69 km, this translates into ~ 6 arcsec accuracy in the pointing direction of the instrument line-of-
70 sight (LOS) with respect to earth's horizon. This is often a difficult if not impossible goal to
71 achieve.

72 In this paper we critically examine the performance of two methods of altitude registration that
73 compare the radiances measured by the instrument to model calculations of radiances. We
74 discuss the methods' inherent strengths and limitations and then assess their performance using
75 data from the OMPS Limb Profiler (LP), launched onboard the Suomi NPP (SNPP) satellite on
76 October 28, 2011.

77 One of these techniques, known as Rayleigh Scattering Attitude Sensing (RSAS), is relatively
78 insensitive to instrument radiometric errors and drift. However, it works best when the effect of
79 aerosols on 350 nm/20 km limb radiances are small. Under these conditions, the accuracy of the
80 method is determined by the accuracy of the geopotential height (GPH) data near 3 hPa (~ 40 km)
81 that is used to calculate the limb radiances. Since aerosol contamination limits the range of
82 latitudes and seasons where RSAS can be applied, we developed the Absolute Radiance Residual
83 Method (ARRM). Although ARRM can be applied more broadly than RSAS, it is more suitable
84 to analyzing relative rather than absolute errors.

85 We describe the theoretical basis of these two techniques in Section 2, and move on to results for
86 the OMPS LP instrument in Section 3. Finally, we present several validations of our uncertainty
87 estimates in Section 4.

88

89 **2 Theoretical Basis**

90 Most scene-based altitude registration methods applied to limb-scattering instruments take
91 advantage of the fact that the atmospheric Rayleigh scattering measured by these instruments
92 varies by 12-14%/km in the absence of particulate scattering from aerosols and clouds and
93 absorption by trace gases. For wavelengths longer than 310 nm, the limb-scattered radiance has a

94 significant contribution from diffuse upwelling radiance (DUR), which is affected by
95 tropospheric clouds, aerosols and surfaces from inside a circular cone whose base extends
96 hundreds of km to the horizon. At non-ozone absorbing wavelengths DUR can be as much as
97 half of the measured radiance. Since DUR is difficult to model accurately, all successful altitude
98 registration methods must be relatively insensitive to variations in it.

99 The RSAS method, described in Sect. 2.1, employs signal ratios in which the DUR effects
100 largely cancel. The ARRM, described in Sect. 2.2, uses 295 nm radiances for which ozone
101 absorption screens the DUR signal. The Knee method, described in Sect. 2.3, has been used
102 extensively by others (Sioris et al., 2003; Kaiser et al., 2004; Rault et al., 2005; von Savigny et
103 al., 2005, Taha et al., 2008), but our analysis indicates that it has no advantages over RSAS and
104 ARRM.

105

106 **2.1 Rayleigh Scattering Attitude Sensor (RSAS)**

107 This technique is named after a sensor that was flown on the Space Shuttle STS-72 in January
108 1996 (Janz et al., 1996) to test the concept originally proposed by one of the authors (Bhartia) ca
109 1992. The technique takes advantage of the fact that change in the log of the limb-scattered (LS)
110 radiance I with altitude z , $d\ln I/dz$, changes by a factor of 3 between 40 km and 20 km for
111 wavelengths near 350 nm (Fig. 1). This is caused by the exponentially increasing attenuation of
112 Rayleigh scattering with pressure. At 40 km this attenuation is small and $d\ln I/dz$ is largely
113 determined by $d\ln P/dz$, where P is the atmospheric pressure at altitude z . However, at 20 km the
114 extinction and scattering nearly cancel where the line of sight (LOS) intersects the Earth radius
115 vector at a right angle, called the tangent point (TP). Therefore the radiances at 20 km are
116 relatively insensitive to the exact altitude of the TP. Though several variations of the RSAS
117 technique have been developed (McPeters et al., 2000; Rault et al., 2005; Taha et al., 2008), we
118 find that the simplest formulation described below works as well as any other.

119 If r is the ratio of radiances for wavelength λ at altitudes z_1 and z_2 , and s_1 and s_2 are the vertical
120 slopes $d\ln I/dz$ at those altitudes, then the error in tangent height (TH) can be calculated as
121 follows:

$$122 \Delta z = - \frac{\ln(r)_m - \ln(r)_c}{s(z_1) - s(z_2)} \quad (1)$$

123 where the subscript m refers to the measured radiance ratios, and c to the ratio calculated using a
124 radiative transfer model. To get the most accurate estimate of TH error the denominator should

125 be as large as possible and the uncertainties in estimating the numerator should be small. The
126 smallest uncertainties in the numerator occur at wavelengths near 350 nm, where trace gas
127 absorption and aerosol scattering effects are small. Setting z_1 to be near 40 km and z_2 to be at or
128 below 20 km maximizes the value of the denominator, typically near 0.10/km. So an accuracy of
129 0.01 (equal to 1% in radiance ratios) is needed to estimate TH within 100 m.

130 As Fig. 2 shows, the largest source of noise in estimating the numerator comes from the
131 mismatch in cloud sensitivity of radiances at the two altitudes. However, this noise is random
132 and can be reduced by averaging data from multiple orbits.

133 Aerosols in the instrument's LOS are a more important source of error. Though the effect of
134 aerosols near 350 nm is small compared to longer wavelengths, it is quite complicated (Fig. 3)
135 and difficult to model since it is determined by subtle differences between two large effects: the
136 reduction of Rayleigh scattering by aerosol extinction and the enhancement of limb radiances by
137 aerosol scattering. In addition, 350 nm LS radiances at 20 km are significantly affected by
138 variation of aerosols along the LOS because of large Rayleigh attenuation; aerosols in the LOS
139 close to the sensor contribute more heavily to the radiance than those far away. Though this
140 effect is similar to the cloud effect mentioned earlier, it is not random because aerosols tend to
141 have systematic latitudinal variability. Given this complexity, the RSAS method works best in
142 latitudes and months where the 350 nm aerosol extinction at 20 km is relatively small.

143 Another potential source of uncertainty in applying the RSAS technique comes from uncertainty
144 in estimating r_c at 40 km; one needs to have accurate pressure profiles at and above 40 km. If the
145 pressure profiles are obtained from geopotential height (GPH) profiles provided by
146 meteorological data assimilation systems, a one-to-one relationship exists between the two errors:
147 a 100 m error in GPH at 3 hPa translates into ~100 m error in determining TH altitude.

148

149 **2.2 Absolute Radiance Residual Method (ARRM)**

150 This method uses radiances measured by a limb instrument near 295 nm at ~65 km to determine
151 altitude error. The main advantage of ARRM is that it reduces aerosol contamination effects
152 because, with the exception of polar mesospheric clouds (PMCs), the atmosphere is typically
153 free of particulate matter at 65 km. PMCs, which form in the polar summer and are typically
154 located at 80 km, can significantly affect 65 km limb radiances if they are in the LOS of the
155 instrument. Fortunately most of the PMC contamination is screened using a 353 nm channel

156 radiance residual flag at 65 km. Though 295 nm radiances are very ozone sensitive, this
157 sensitivity drops to less than 0.2% for a 10% change in ozone above 65 km. This sensitivity can
158 be accounted for by using climatological ozone profiles.

159 The principal difficulty in applying ARRM comes from the fact that one cannot get accurate
160 GPH data near 0.1 hPa needed to calculate 295 nm radiances at 65 km. To reduce this error we
161 developed a variation of a technique that has been used for many years to derive mesospheric
162 temperature profiles from the vertical slope of Rayleigh-scattered radiances measured by ground-
163 based UV lidars (McGee et al., 1991). Though it may be possible to derive temperature profiles
164 using 350 nm limb radiances, we are more interested in using the vertical slope of Rayleigh-
165 scattered radiances to correct the 295 nm radiance residuals calculated using meteorological data.
166 The residual at wavelength λ at altitude z , defined as $d(\lambda,z) = \ln I_m(\lambda,z) - \ln I_c(\lambda,z)$, is corrected
167 using 350 nm residuals:

$$168 \quad d_{corr}(\lambda, z) = d(\lambda, z) - [d(350, z) - d(350, z_0)] \quad (2)$$

169 where z_0 is a normalization altitude.

170 The 350 nm differential residuals on the right side provide an estimate of the relative error in
171 calculating radiances using meteorological data between z and z_0 . Since this error should be
172 wavelength independent, we can use this term to correct the residuals at any wavelength,
173 assuming that the meteorological data at z_0 is accurate and that the 350 nm wavelength is well
174 calibrated. The large response of OMPS LP at 350 nm results in signals that are the least affected
175 by out-of-band stray light.

176 The TH error estimated using this method is given by:

$$177 \quad \Delta Z = \frac{d_{corr}(\lambda, z)}{s(\lambda, z) - [s(350, z) - s(350, z_0)]} \quad (3)$$

178 We are minimizing ozone profile sensitivity by applying this method to radiances at wavelengths
179 shorter than 300 nm. At longer wavelengths DUR makes the LS radiances sensitive to total
180 column ozone at all altitudes. At 295 nm, the use of z near 65 km provides low ozone sensitivity.
181 Though it is best to set z_0 as low as possible to minimize GPH caused errors, aerosol
182 contamination limits the value to around 40 km.

183 ARRM has two primary uncertainties. Since 1% error in radiance calibration produces ~ 70 m
184 error in determining the TH, this method requires accurate radiances (or sun-normalized
185 radiances) and may be affected by instrument degradation. Though the absolute accuracy of

186 ARRM may not be as good as RSAS, this method can be applied at latitudes/seasons where
187 RSAS cannot be applied reliably because of aerosol contamination. And like RSAS, this method
188 is also sensitive to errors in GPH profile near 3 hPa, which are used for calculating 350 nm
189 radiances at 40 km.

190

191 **2.3 “Knee Method”**

192 The name of this method is derived from the characteristic knee shape of the limb radiance
193 profiles (Fig. 4). Above the knee the radiances decrease with altitude due to exponential decrease
194 in Rayleigh scattering and ozone density. Below the knee the ozone absorption becomes so large
195 that it essentially blocks most of the Rayleigh-scattered radiation from reaching the satellite,
196 making the radiances insensitive to atmospheric pressure. This characteristic shape allows one to
197 estimate altitude registration error in a manner very similar to that of RSAS. The principal
198 advantage of this method is that one can use shorter wavelengths where aerosols are not a
199 problem. However, this comes at a penalty; the method requires accurate ozone and pressure
200 profiles near and above the knee region. Radiative transfer calculations using climatological
201 ozone profiles indicate that a 10% error in assumed ozone density (at all altitudes) will produce
202 about a 250 m error in altitude registration (Fig. 5). The method also has a sensitivity to GPH
203 errors that is similar to RSAS and ARRM. In our view this method provides no compelling
204 advantage over comparing the ozone profiles retrieved from a limb scattering sensor with other
205 ozone sensors to determine altitude registration errors. Indeed, such direct ozone comparisons are
206 simpler and more reliable if the altitude registration error is the largest error source, and we use
207 this technique to evaluate the results of RSAS and ARRM in Sect. 3.

208

209 **3 Results**

210 In this section we discuss altitude registration errors in OMPS LP radiances determined first by
211 “Slit Edge” analysis of the instrument focal plane image and then by the application of the RSAS
212 technique. The remaining errors are analyzed using ARRM.

213

214 **3.1 Slit Edge Results**

215 The OMPS LP sensor utilizes a two-dimensional charge coupled device (CCD) detector to
216 capture spectrally dispersed (along the 740 pixel row dimension) and vertically distributed (along

217 the 340 pixel column dimension) radiation (Fig. 6). Three long vertical entrance slits spaced 4.25°
218 apart produce three distinct images of the atmosphere that are collected simultaneously on the
219 single CCD. The resulting limb radiance profile from the center slit is aligned very closely to the
220 satellite ground track with tangent points trailing approximately 3000 km south of the sub-
221 satellite point. The east and west slit images are separated in longitude by 2.25° (250 km at their
222 tangent points) from that of the center slit.

223 An unexpected thermal sensitivity was discovered in the LP instrument soon after launch (Jaross
224 et al., 2014). Expansion of the LP instrument's entrance baffle as the sun illuminates it midway
225 through the northern hemisphere causes mirrors in the telescope to rotate slightly, which in turn
226 moves the limb radiance image on the detector. Since there are separate mirrors for each entrance
227 slit, the three slit images move independently. These image motions cause misregistration of
228 both the vertical pointing and center wavelength of each pixel. Vertical pointing changes are
229 detected most clearly by observing the location (detector column) of the lower slit edge, which
230 has a sharp signal gradient. Figure 7 contains plots of the average edge locations in the vertical
231 (altitude) dimension along the orbit. These pointing shifts are very repeatable (ranging only ± 15
232 m at a given point in the orbit over a year).

233 Since the same slit edge analysis can be applied to pre-launch test data, it is possible to obtain the
234 pixel line of sight shift relative to its calibrated value in the spacecraft reference frame. There is
235 no evidence of image distortion so this shift is the same for all detector pixels within a slit image.
236 The edge analysis indicates the three slit edges shifted by the equivalent of 570/470/950 m
237 (east/center/west slits, respectively) at the middle of an orbit relative to pre-launch measurements.
238 A mean sensor temperature decrease exceeding 25°C from ground to on-orbit conditions is the
239 suspected cause. We believe there are no additional uncorrected pointing shifts arising from
240 within the LP instrument. An error or change in the alignment of the instrument with respect to
241 S/C axes is not detectable using this method.

242

243 **Section 3.2 RSAS results**

244 We use the radiative transfer code described by Loughman et al. (2015) to estimate 350 nm
245 radiances. Since the 40/20 km radiance ratio is not sensitive to polarization effects, we use the
246 faster scalar code rather than the full vector one to calculate DUR. The calculations are done
247 assuming a pure Rayleigh atmosphere bounded by a Lambertian reflecting surface at 1013.25

248 hPa. The reflectivity of this surface is calculated using limb measurements at 40 km. However,
249 both measurements and calculations show that the ratio of 40/20 km radiances is not affected by
250 reflectivity or surface pressure and there is no discernible cloud effect. Since NO₂ only has a
251 very small (<0.5%) effect on 350 nm radiances, climatological NO₂ profiles are used in the
252 calculation. We use OMPS LP retrieved ozone profiles. The RSAS analysis is not sensitive to
253 ozone assumptions because it uses the ozone insensitive 350 nm radiances.

254 We estimate pressure and temperature versus altitude at the LP measurement locations and time
255 from the Modern-Era Retrospective Analysis for Research and Application (MERRA) data
256 (GEOS-5 FP_IT Np) from the Global Modeling and Assimilation Office (GMAO) at NASA
257 Goddard Space Flight Center (GSFC). The data are provided as geopotential heights (GPH) at 42
258 pressures from the surface to 0.1 hPa, on a 0.5° latitude x 0.625° longitude horizontal resolution
259 grid, and at a 3 hour interval. The GPH is converted to geometric height using a standard formula
260 that takes into account the variation of gravity with latitude and elevation.

261 As discussed in Sect. 2.1, RSAS results are affected by aerosols near 20 km. Aerosol profiles
262 derived from the Optical Spectrograph and InfraRed Imaging System (OSIRIS) data (Llewellyn
263 et al, 2004; Bourassa et al, 2007) indicate that tropical aerosols reached a minimum value (during
264 the OMPS lifetime) just before the eruption of the Kelud volcano in Indonesia on February 14,
265 2014 (Fig. 8). We have therefore chosen to use equatorial RSAS data before the eruption to
266 estimate the altitude registration errors (listed in Table 1). These TH errors range between ~1 and
267 ~1.5 km for the three slits, and have been applied to the Version 2 OMPS LP Ozone data set.
268 Radiative transfer calculations using OSIRIS-derived aerosol profiles indicate that the aerosol
269 caused errors in the results shown are less than 100 m.

270

271 **Section 3.3 ARRM results**

272 We utilized the same radiative transfer code and profile inputs used for RSAS to calculate
273 radiances at 295 nm. Ozone concentrations from the OMPS LP retrievals were used. As
274 mentioned previously, though 295 nm radiances are very ozone sensitive, this sensitivity drops to
275 less than 0.2% for a 10% change in ozone above 65 km. As discussed in Sect. 2.2, the absolute
276 accuracy of ARRM may not be as good as RSAS, but this method can be applied at latitudes and
277 seasons where RSAS cannot be applied reliably because of aerosol contamination.

278 Time dependent plots (Fig. 9) show negative pointing trends of approximately 100 m over the
279 four years of data, and even larger seasonal variations depending on the latitude band and slit
280 over the four years of data. Much of this trend is the result of a 6 arcsec (a TH change of ~100m)
281 spacecraft pitch adjustment that occurred on 25 April 2013. Figure 9 clearly shows this abrupt
282 change.

283 The largest disagreement between the 3 slits (~400 m) occurs in the high northern hemisphere. In
284 the southern hemisphere the disagreement is closer to 100 m. In addition we see ± 200 m
285 seasonally varying errors that could be due to either true pointing changes or errors in the GPH
286 data that we used in our analysis. Such variations in 295 nm radiances cannot be explained by
287 known seasonality in ozone concentration at 65 km.

288 The ARRM method is designed to accommodate stray light errors that are independent of
289 wavelength. No additional TH errors occur when stray light at 65km is the same at 295 and
290 350nm. The ground characterization of Limb sensor stray light indicates a small wavelength
291 dependence (Jaross, 2014), and this is removed in ground processing. Our subsequent
292 comparisons with RTM predictions indicate that residual stray light errors at 65 km have a daily
293 mean bias that translates to less than 100 meters in TH.

294 The ARRM analysis shows a distinct latitude dependence (Fig. 10) with some seasonal
295 differences. While it is tempting to attribute this entirely to TH error, we conservatively do not
296 apply the ARRM results to our data since the uncertainties are of the same magnitude. As with
297 RSAS, this method is sensitive to errors in GPH profile near 3 hPa used for calculating 350 nm
298 radiances at 40 km (see Sect. 4.1). Further analysis is needed to determine the precise cause of
299 the remaining errors.

300

301 **Section 4 Validation**

302 In this section we consider uncertainties in the parameters used to derive TH errors to indirectly
303 validate the results shown in Sect. 3, and to estimate the remaining uncertainties in the LP TH
304 due to errors in these parameters. Section 4.1 focuses on the validation of 3 hPa GPH
305 information from MERRA that was assumed as the truth in our calculations. In Section 4.2 we
306 consider the reflectivity measured by the OMPS nadir sensor to validate LP-measured radiances
307 at 350 nm, which vary by $\sim 14\%/km$ near 40 km. Finally, in Sect. 4.3 we compare the LP-derived

308 ozone mixing ratio at 3 hPa with the Microwave Limb Sounder (MLS). For the validation studies
309 in this section, the OMPS LP TH has been corrected with the errors listed in Table 1.

310

311 **Section 4.1 GPH comparison**

312 Errors in the GPH profile assumptions directly translate into TH errors. Although the 3hPA GPH
313 varies over 4 km along an orbit, a comparison of daily averaged values from MLS and MERRA
314 show differences that are usually less than 200 m (Fig. 11). These differences do not directly
315 explain the latitude dependence of TH errors shown in Fig. 10, but do provide an estimate of the
316 magnitude of errors caused by the use of MERRA GPH in our radiative transfer calculations.
317 Better agreement seen at the poles may simply be due to the fact that there are not many
318 measurements at these latitudes and both may be influenced by the same climatology. As a result,
319 it is not clear how these GPH errors influence the ARRM results. However, in Section 4.3 we
320 discuss some suggestive but inconclusive results untangling GPH errors from TH errors.

321

322 **Section 4.2 Radiances comparison**

323 We previously described (in Section 2) the difficulty modeling DUR caused by scene
324 heterogeneity and aerosols. Both the RSAS method and ARRM depend upon an accurate model
325 for DUR at 40 km relative to other altitudes, and any model errors translate directly (Equations 1
326 and 3) into false estimates in the TH errors.

327 We estimate the DUR modeling error by comparing LP measured and modeled 353 nm radiances
328 at 3 hPa. The radiances are modeled using an independent, nearly simultaneous measure of
329 reflectivity from the surface-atmosphere system derived from the OMPS Nadir instrument at 340
330 nm. The reflectivity derived from the 50x50 km nadir-view measurements are relatively
331 insensitive to DUR effects (compared to reflectivity derived from the LP measurements). With
332 better reflectivity assumptions the model/measurement comparisons offer a lower bound of the
333 effect of DUR modeling errors.

334 The radiance comparison, shown in Fig. 11, suggests model or calibration errors of 2-3% on
335 average, plus structures caused by the limb and nadir scene mismatch. If this error were
336 attributed solely to the limb modeled DUR effect, the resulting TH error would be less than +/-
337 200 m. There is no evidence of either a seasonal or a latitude dependence in the four days of

338 comparisons, meaning that DUR effects cannot explain the robust seasonal and latitudinal
339 variations seen in ARRM results (Fig. 9 and Fig. 10). These model/measurement comparisons
340 provide an estimate of errors related to incomplete modeling of DUR and inhomogeneous
341 surface albedo included in our RSAS and ARRM results. We therefore conclude those variations
342 arise from errors in the GPH scale or from true TH variations.

343

344 **Section 4.3 Ozone comparison**

345 At 3 hPa limb ozone retrievals are very sensitive to TH errors, with 20 to 25% per km change in
346 ozone concentration (see Fig. 5). Similar to the Knee Method, we can use this sensitivity to
347 gauge the residual TH errors. We compare LP ozone retrievals against Aura MLS v4 ozone
348 retrievals at 3 hPa (near 40 km) (Fig. 13). While the latitudinal patterns of differences
349 significantly vary with season, we find agreement within $\pm 10\%$ over all seasons and latitude
350 bands. If completely interpreted as due to TH error, a 10% difference would translate to less than
351 500 m error. These comparisons confirm a residual uncertainty in our scene-based altitude
352 registration techniques of $\pm 200\text{m}$.

353 The ARRM method has displayed the ability to track any drifts or sudden changes of 50 m (Sect.
354 3.3), and time series of TH error derived from the ARRM method track very closely to the time
355 series of the LP/MLS 3 hPa ozone differences (Fig. 14). The highest correlation (0.76) was found
356 at 45° south latitude, with considerable smaller values in the northern hemisphere (0.30 at 60°
357 north). Whether this suggests the ARRM results can be attributed solely to TH errors has not
358 been determined yet.

359 Both ARRM and LP/MLS ozone comparison depend upon accurate TH and MERRA
360 information, and in the same way. So, while these results suggest some confidence in the
361 ARRM technique, we cannot assign the correlation shown in Fig. 14 to only a TH error or a
362 MERRA error. It is important to note that MLS ozone profiles are reported as volume mixing
363 ratio on a vertical pressure grid, while the LP algorithm retrieves ozone as number density on an
364 altitude grid. Thus, in order to compare LP and MLS ozone retrievals we had to convert ozone
365 units using MERRA temperature and GPH profiles. This conversion inevitably introduces errors
366 in MERRA GPH into the ozone comparisons. Therefore ozone differences between LP and MLS
367 ozone retrievals not only depend on the LP TH error, but on errors in MERRA GPH as well as
368 on errors in the retrieval algorithms and instrumental sampling (geophysical noise). Furthermore,

369 analysis of LP and MLS ozone retrievals indicates a large daily ozone variability within a 5-
370 degree latitude bin at 3 hPa that ranges from 2% in the tropics to 20% at high latitudes with the
371 seasonal maximum during austral winters (results are not shown here), which can give readers a
372 sense of geophysical ozone variability. In consideration of all of the above factors, we remain
373 cautious in making definite conclusions and applying time-dependent corrections for the LP TH
374 at this time; further analysis and comparisons with independent ozone observations (like SAGE
375 III) are needed to confirm the results.

376

377 **Section 5 Conclusions**

378 Accurate altitude registration is key to the success of the limb scattering measurement
379 technique. We have described two scene-based techniques that together provide highly precise
380 and accurate estimates of the tangent height. These altitude registration techniques are
381 inexpensive and more comprehensive than external sources of attitude information, such as star
382 trackers mounted on the spacecraft. Though star trackers are highly accurate devices, translation
383 of that accuracy to the limb scene is also not without uncertainty, as we have seen with the SNPP
384 spacecraft. Though we were able to calibrate thermal sensitivities within the OMPS instrument,
385 we have yet to identify the source of 1-1.5 km pointing errors derived from RSAS (see Table 1).
386 These may arise from mounting offsets of the instrument and star trackers, or from spacecraft
387 flexure between the two.

388 The RSAS and ARRM techniques are complementary because the former is
389 accurate to ± 200 m, but only under limited conditions. The accuracy of
390 ARRM cannot be easily established, but it has a precision also within
391 ± 200 m. We believe this results in small, less than 100 m, trend
392 uncertainties for sufficiently long time series, as demonstrated by the
393 OMPS ARRM record.

394 The single largest source of uncertainty in both techniques is knowledge of the atmospheric
395 pressure vertical profile, which must be provided from external sources. Given uncertainties in
396 GPH data, as seen in the MLS comparison, as both well as uncertainties in our ozone retrieval
397 algorithm (not related to TH error), it is currently not possible to tell if the latitudinal and
398 seasonal variations seen in ARRM results are caused by TH error. Further work will be needed
399 to understand their cause. We have shown, however, that ARRM is capable of multi-year trend

400 uncertainties that are on the order of 100m or smaller. Furthermore, the two TH registration
401 methods discussed in the paper allow us to track any drifts or sudden changes in our altitude
402 registration to better than 50 m, which is the minimum level necessary to derive accurate ozone
403 trends from a limb technique.

404

405

406

407 Acknowledgements: The authors gratefully acknowledge the assistance of NASA's Limb
408 Processing Team in providing the data used in this paper. We would also like to thank Dave
409 Flittner, Ernest Nyaku and Didier Rault, helped with the development and updates of the RT
410 model. Finally, we'd like to acknowledge the role Didier played in laying the groundwork for the
411 OMPS limb retrieval algorithm

412

413

414 **References**

415 Bourassa, A. E., Degenstein, D. A., Gattinger, R. L., and Llewellyn, E. J.: Stratospheric aerosol
416 retrieval with optical spectrograph and infrared imaging system limb scatter measurements, *J.*
417 *Geo-phys. Res.*, 112, D10217, doi:10.1029/2006JD008079, 2007.

418

419 Jaross, G., P. K. Bhartia, G. Chen, M. Kowitt, M. Haken, Z. Chen, P. Xu, J. Warner, and T.
420 Kelly: OMPS Limb Profiler instrument performance assessment, *J. Geophys. Res. Atmos.*, 119,
421 doi:10.1002/2013JD020482, 2014.

422

423 Janz, S. J., E. Hilsenrath, D. E. Flittner, and D. F. Heath, Rayleigh scattering attitude sensor,
424 *Proc. SPIE 2831, Atmospheric Ultraviolet and Space Remote Sensing: Methods and*
425 *Instrumentation*, 146, doi:10.1117/12.257207, 1996.

426

427 Kaiser, J. W., C. Von Savigny, K.-U. Eichmann, S. Noel, H. Bovensmann, and J. P. Burrows,
428 *Satellite-pointing retrieval from atmospheric limb-scattering of solar UV-B radiation*, *Can. J.*
429 *Phys.*, 82, 1041-1052, 2004.

430

431 Llewellyn, E. J., N. D. Lloyd, D. A. Degenstein, R. L. Gattinger, S. V. Petelina, A. E. Bourassa,
432 J. T. Wiensz, E. V. Ivanov, I. C. McDade, B. H. Solheim, J. C. McConnell, C. S. Haley, C. von
433 Savigny, C. E. Sioris, C. A. McLinden, E. Griffioen, J. Kaminski, W. F. Evans, E. Puckrin, K.
434 Strong, V. Wehrle, R. H. Hum, D. J.W. Kendall, J. Matsushita, D. P. Murtagh, S. Brohede, J.
435 Stegman, G. Witt, G. Barnes, W. F. Payne, L. Piche, K. Smith, G. Warshaw, D. L. Deslauniers,
436 P. Marc-hand, E. H. Richardson, R. A. King, I. Wevers, W. McCreath, E. Kyrölä, L. Oikarinen,
437 G. W. Leppelmeier, H. Auvinen, G. Megie, A. Hauchecorne, F. Lefevre, J. de La Noe, P.

438 Ricaud, U. Frisk, F. Sjoberg, F. von Scheele, and L. Nordh: The OSIRIS instrument on the
439 Odin spacecraft, *Can. J. Phys.*, 82, 411–422, 2004.
440

441 Loughman, R., D. Flittner, E. Nyaku, and P. K. Bhartia, Gauss–Seidel limb scattering (GSLs)
442 radiative transfer model development in support of the Ozone Mapping and Profiler Suite
443 (OMPS) limb profiler mission, *Atmos. Chem. Phys.*, 15, 3007-3020, 2015.
444

445 McGee, T. J., D. Whiteman, R. Ferrare, J. J. Butler, and J. Burris, STROZ LITE: Stratospheric
446 ozone lidar trailer experiment, *Opt. Eng.*, 30, 31-39 (1991).
447

448 McPeters, R. D., S. J. Janz, E. Hilsenrath, T. L. Brown, D. E. Flittner, and D. F. Heath, The
449 retrieval of O₃ profiles from limb scatter measurements: Results from the Shuttle Ozone Limb
450 Sounding Experiment, *Geophys. Res. Lett.*, 27, 2597-2600, 2000.
451

452 Rault, D.F., Ozone profile retrieval from Stratospheric Aerosol and Gas Experiment (SAGE III)
453 limb scatter measurements, *J. Geophys. Res.*, 110, D09309, doi:10.1029/2004JD004970, 2005.
454

455 Sioris, C. E., et al., Stratospheric profiles of nitrogen dioxide observed by Optical Spectrograph
456 and Infrared Imager System on the Odin satellite, *J. Geophys. Res.*, 108(D7), 4215,
457 doi:10.1029/2002JD002672, 2003.
458

459 Taha, G., G. Jaross, D. Fussen, F. Vanhellemont, E. Kyrölä, and R. D. McPeters, Ozone profile
460 retrieval from GOMOS limb scattering measurements, *J. Geophys. Res.*, 113, D23307,
461 doi:10.1029/2007JD009409, 2008.
462

463 von Savigny, C., J. W. Kaiser, H. Bovensmann, J. P. Burrows, I. S. McDermid, and T. Leblanc
464 (2005), Spatial and temporal characterization of SCIAMACHY limb pointing errors during the
465 first three years of the mission, *Atmos. Chem. Phys.*, 5, 2593-2602, doi:10.5194/acp-5-2593-
466 2005.
467
468
469
470
471
472
473
474
475

476 Table 1: RSAS results at the equator before the Kelud eruption 2014 February. The time period
477 had a minimum value (during OMPS life time) and was chosen using OSIRIS measurements
478 (Fig.8).

TH error, km	EAST	CENTER	WEST
RSAS results	1.12	1.37	1.52

479

480

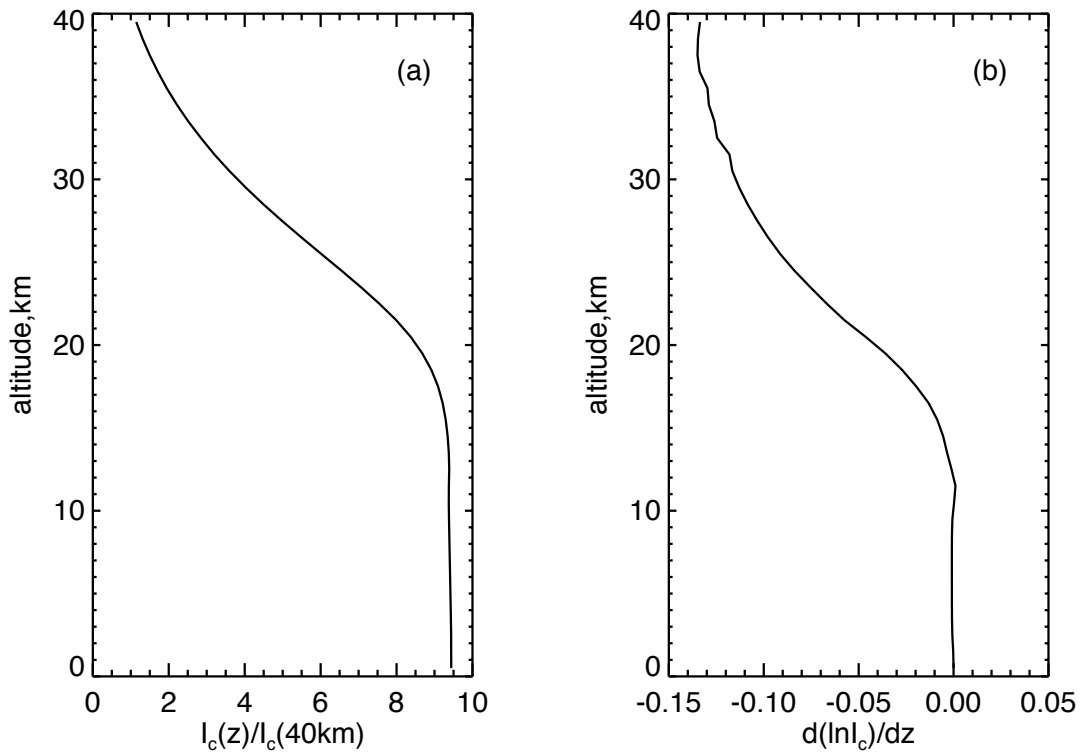


Figure 1: Figure a shows calculated 350 nm radiances as a function of altitude, normalized to 40.5km. The calculation models the OMPS LP field of view and includes no aerosols. The shape of the curve is caused by competition between molecular scattering, which increases roughly linearly with pressure, and attenuation which becomes important when the Rayleigh optical thicknesses near the tangent point starts to become large. Attenuation causes the slope of 350 nm radiances to change sharply between 40 and 20 km (Fig. 1b). Since the ratio of 40 to 20 km radiances at 350 nm varies by 8-10%/km, one can estimate altitude registration errors by comparing measured ratios with ratios calculated using meteorological data.

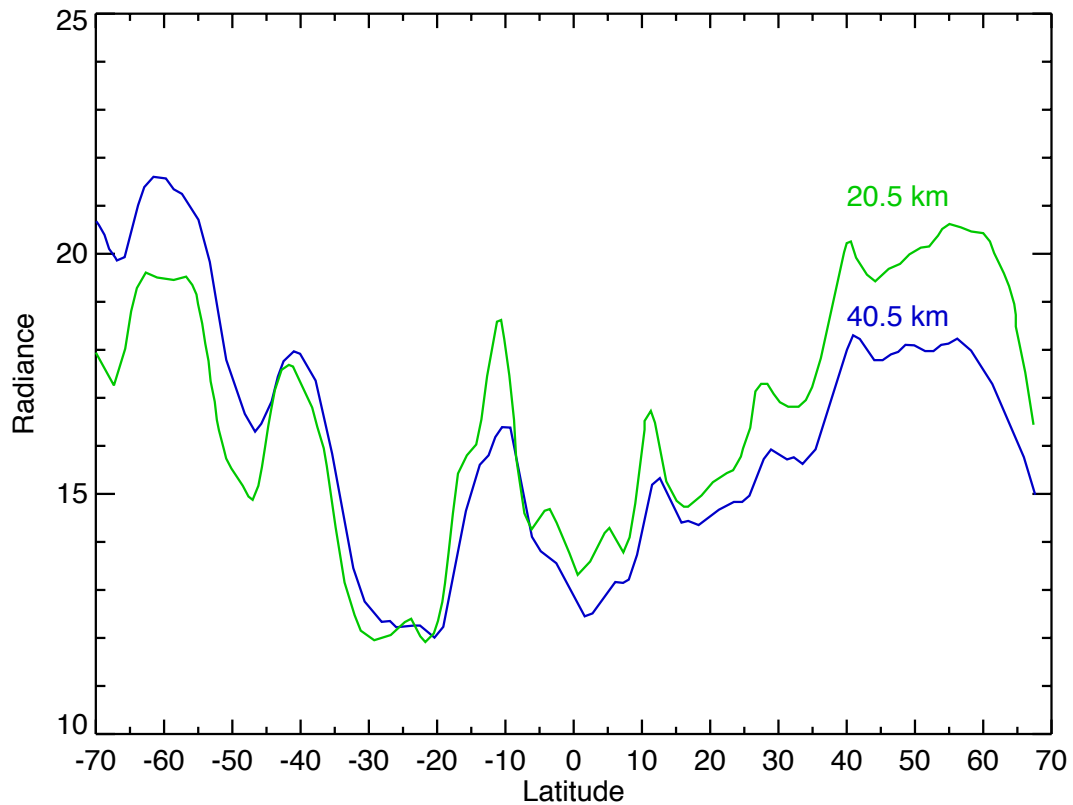


Figure 2: The 353 nm sun-normalized radiances from one orbit of OMPS LP (central slit) taken on Feb. 2, 2012. The blue line shows 40.5 km values and the green line shows 20.5 km values (divided by 8 to put both curves on a similar scale) versus latitude. Since the global aerosol loading on this day was small, the short scale features in both curves are largely caused by variations in cloud and surface albedo. The 20.5 km curve has sharper features and appears to be shifted towards toward the South Pole. This is because large Rayleigh attenuation at 20.5 km causes the radiances to have much higher sensitivity to the atmosphere on the satellite side of the tangent point (TP), while 40.5 km radiances have similar sensitivities to both sides. This effect creates large noise in applying the RSAS technique to orbital data. However, since the noise varies randomly from orbit to orbit, it can be reduced by averaging data from multiple orbits. Figure 6 of Loughman et al. (2015) is an example of how the contributions become asymmetric about the tangent point at lower THs.

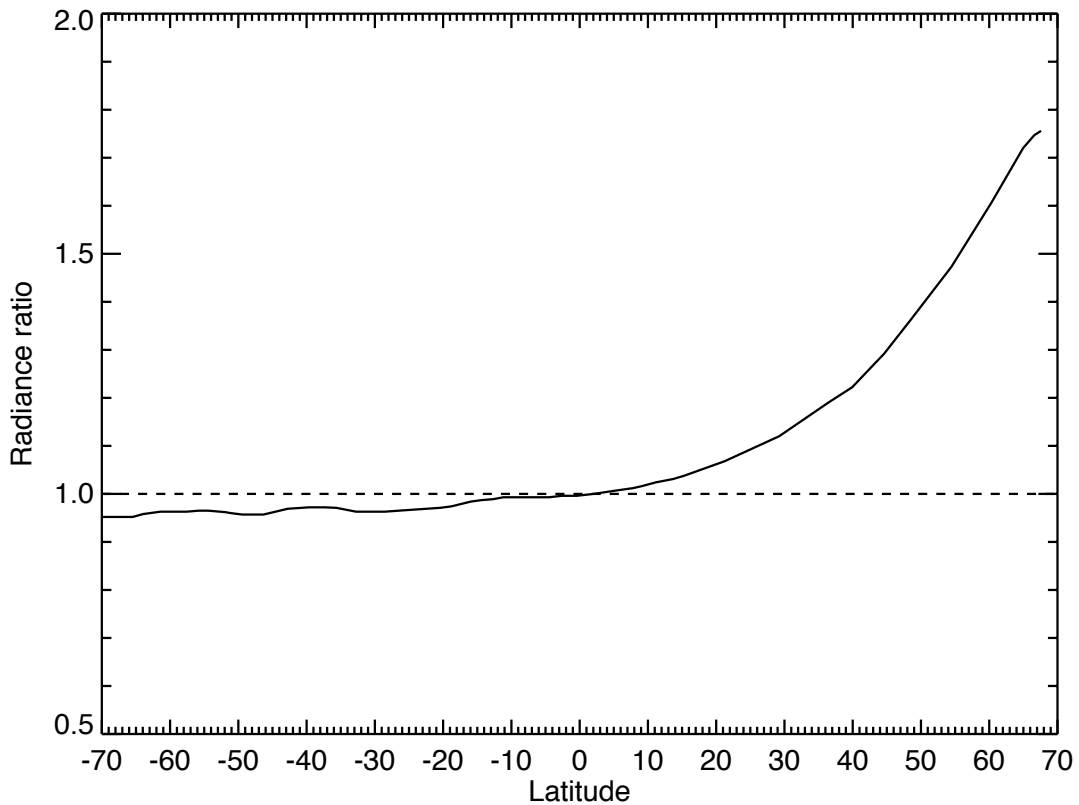


Figure 3: The ratio of 353 nm limb-scattered radiances at 20.5 km with and without aerosols as a function of latitude. A nominal latitude-independent aerosol extinction profile was used in the calculation for the OMPS LP viewing geometry on Feb 2, 2012. The strong latitude dependence is caused by an order of magnitude change in aerosol scattering phase function with latitude combined with the attenuation of Rayleigh-scattered radiation by aerosols along the line-of-sight (LOS). In the southern hemisphere, where LP measures aerosols in the backscatter direction, the latter effect dominates and the radiation decreases. The net effect is very sensitive to altitude, variation of aerosol extinction profile along the LOS, and aerosol particle size distribution, and is therefore difficult to calculate accurately.

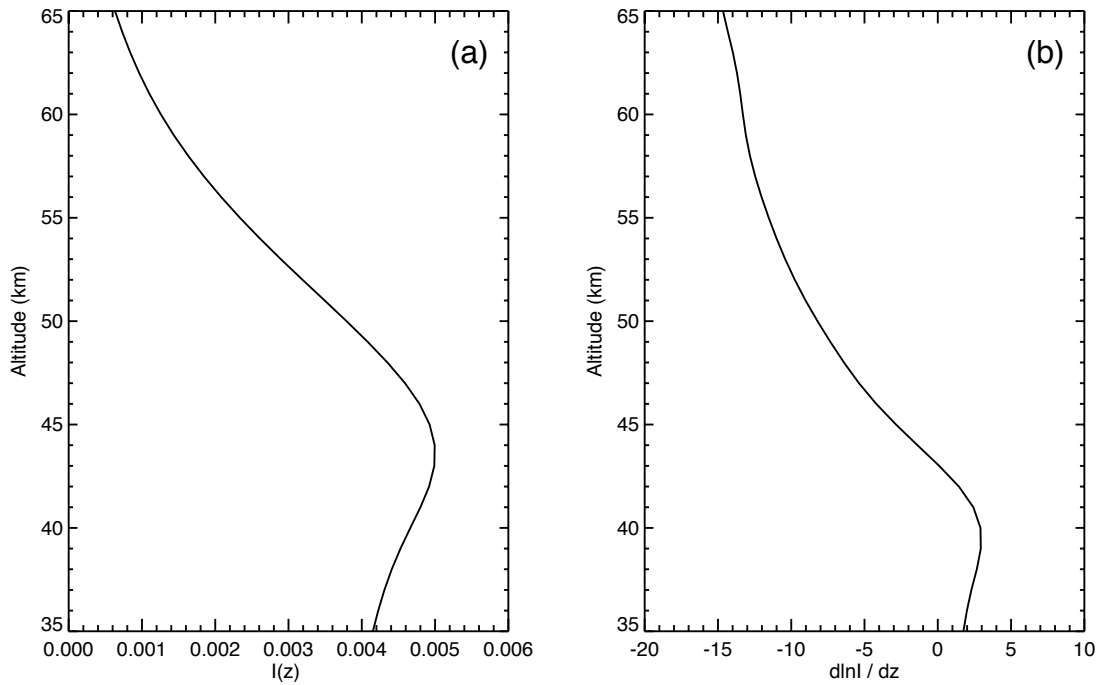


Figure 4: Figure a shows calculated 305 nm radiances assuming no aerosols as a function of altitude. The slope (Fig. 4b) is caused by competition between Rayleigh scattering and ozone absorption near the altitude of maximum radiance, ~44 km. Above 55 km the sensitivity is nearly constant in height, ~13%/km at 65 km. Above the knee the radiances decrease with altitude due to the exponential decrease in Rayleigh scattering and ozone density. Below the knee the ozone absorption becomes so large that it essentially blocks most of the Rayleigh-scattered radiation from reaching the satellite, making the radiances insensitive to atmospheric pressure. This characteristic knee shape allows one to estimate altitude registration error in a manner very similar to that of RSAS, but also makes it very susceptible to ozone profile assumptions, as illustrated in Fig. 5.

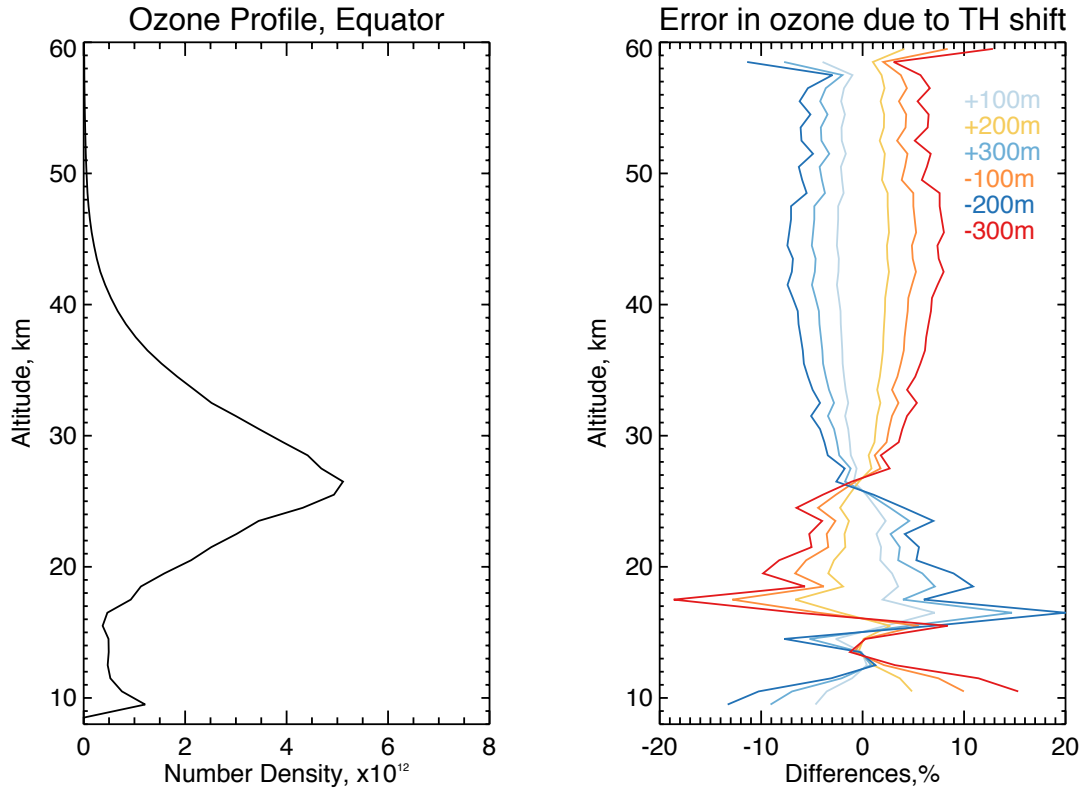


Figure 5: Typical ozone profile in the tropics (left panel) which peaks between 25 and 30 km. By shifting the ozone profile we can estimate an order and pattern of error in ozone profiles due to TH shift (right panel). Errors in ozone retrievals are within 8% at 40 km from TH errors of 300 m. Errors are least sensitive at the ozone peak, and are more variable below.

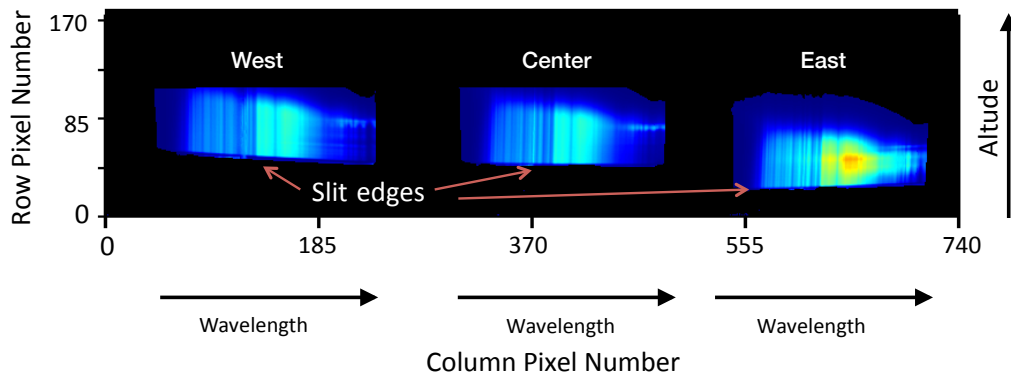


Figure 6: OMPS LP CCD high gain earth viewing radiance images for the 3 slits. The wavelength range for each image is 270 to 1050 nm and the minimal altitude range is 0 to 80 km. The CCD has 740 pixels in the wavelength dimension. There are 340 pixels in the spatial dimension; the high gain images occupy the lower half of the CCD (pixels 0 to 170). The spatial extent of each slit's image on the detector is limited by the vertical length of that slit. The lower slit edges (nearest the Earth surface) provide a high contrast signal cutoff that can be monitored for movement.

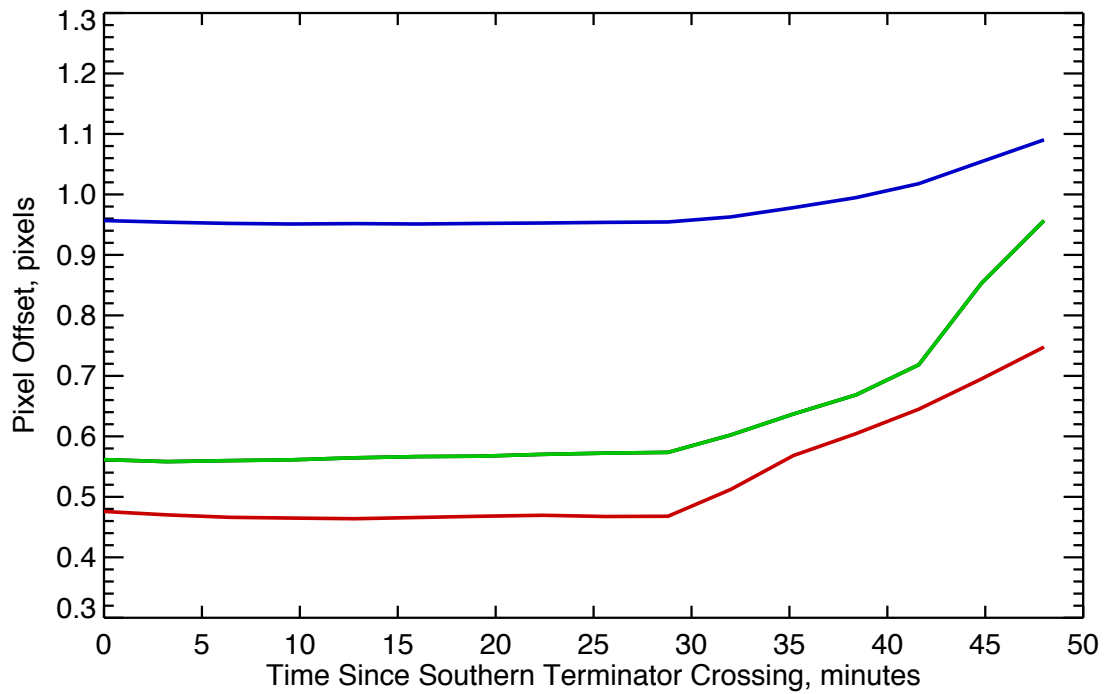


Figure 7: Slit edge results for the three slits (Green=East Slit, Red=Center Slit, Blue=West Slit) plotted against time since Southern Terminator crossing. A 1 pixel shift corresponds to a 965 m TH shift. The offsets are stable from the southern terminator to the mid latitude northern hemisphere where the exposure to the sun increases thermal effects.

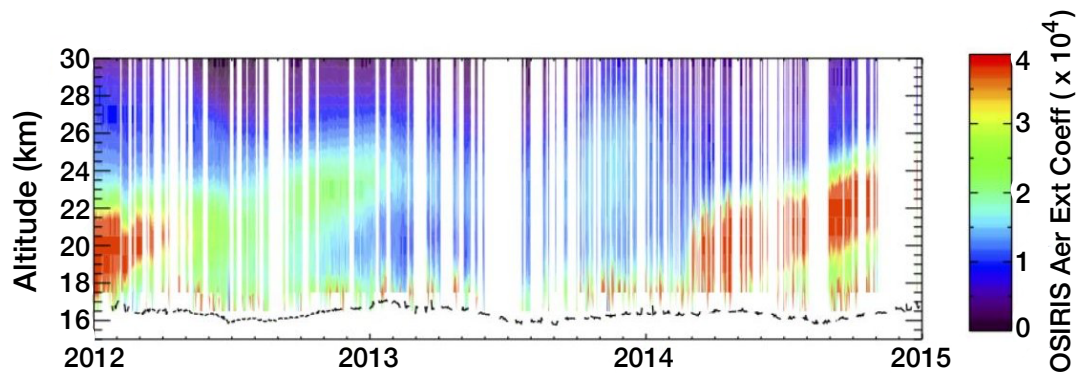


Figure 8: Time series of OSIRIS aerosol extinction profiles above the tropopause (dashed line). The large concentration in 2012 are due to the June 2011 Nabro eruption in Eritrea. The aerosols at 20 km reached a minimum value (during OMPS life time) just before the eruption of the Kelud Volcano on 14 February 2014.

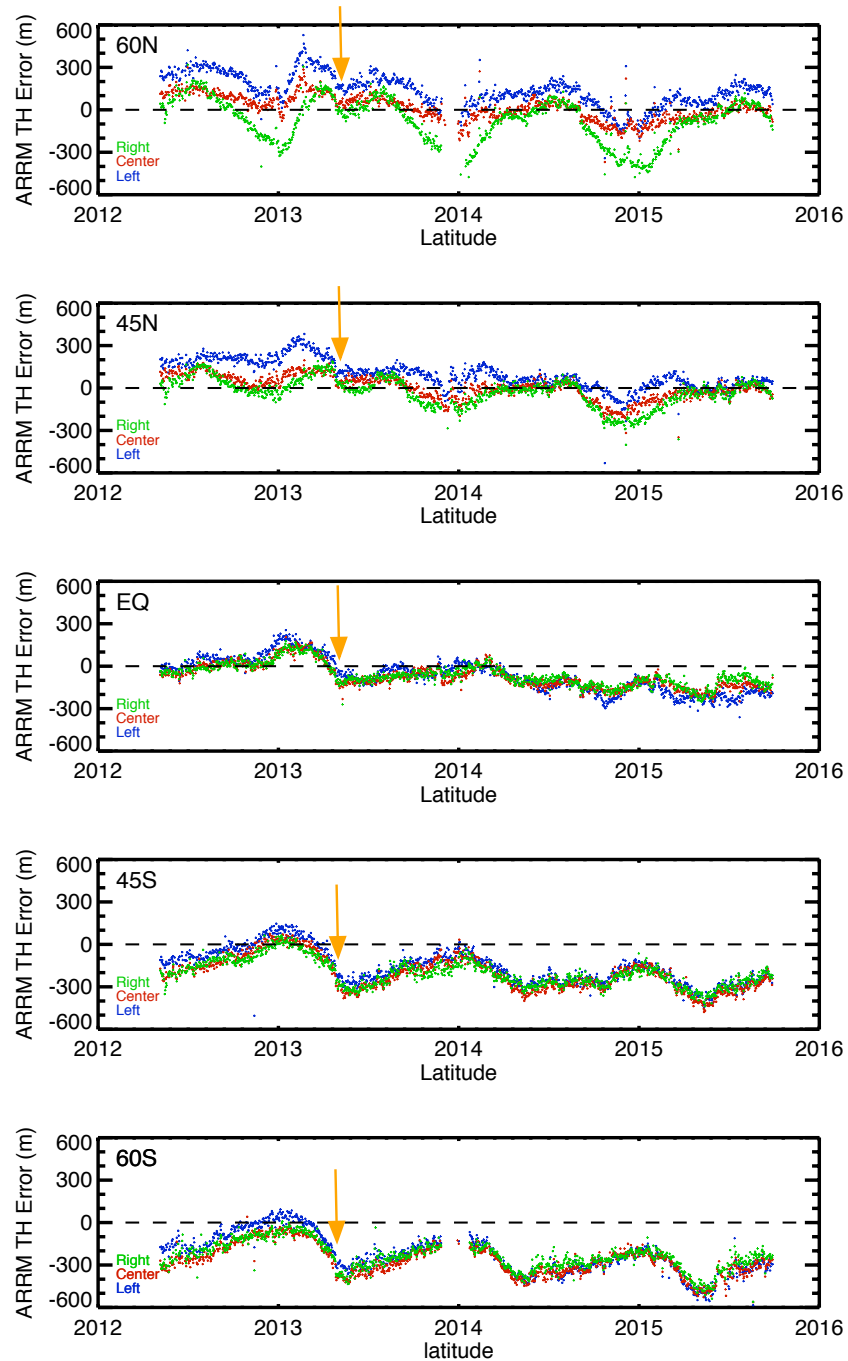


Figure 9: Time dependent plots of TH errors from ARRM analysis at 5 latitude bands for the 3 slits. Values are normalized at the Equator just prior to the Kelud eruption on February 14, 2014 based on the RSAS results summarized in Table 1. Arrows indicate a 12 arcsec pointing adjustment to one of the two spacecraft star trackers on April 25, 2013. The resulting 100 m TH shift can be seen most clearly by comparing 2012 and 2013 results. Slit discrepancies and seasonal dependencies of ± 200 m can also be seen.

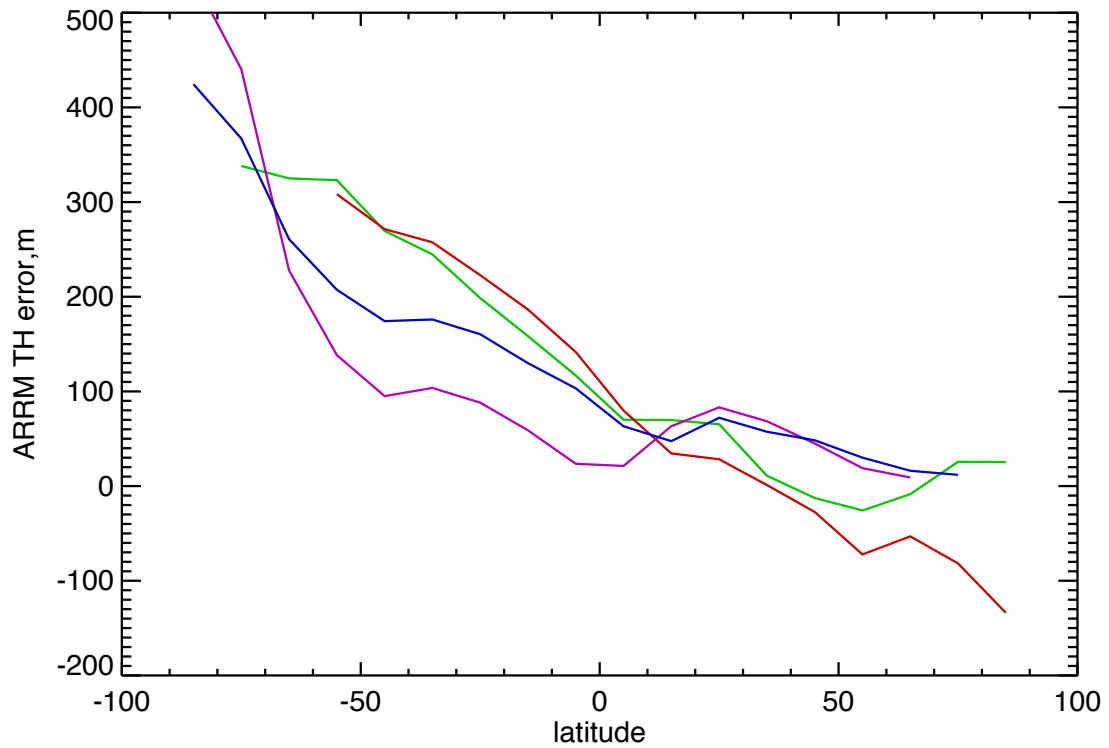


Figure 10: Average (over the ~4 year study period) ARRM results by latitude and seasons (MAM-green, JJA-red, SON-purple, DJF-blue) for Center Slit. On average, excluding the extreme polar regions there appears to be a 300 m TH change over an orbit.

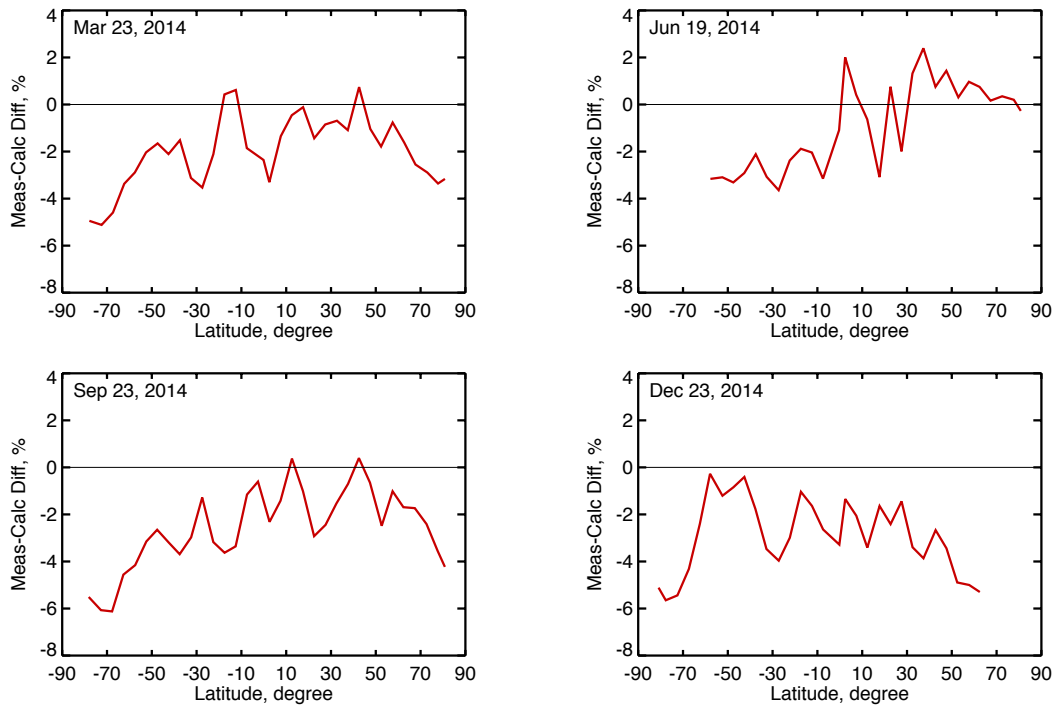


Figure 11: Daily 5 degree zonal means of GPH from MLS (blue), GMAO (green), and the difference MLS-GMAO (red) at 3 hPa GPH for four cardinal days. Note that despite a 2 to 4 km change over an orbit, the differences are generally within 200 m. These differences provide an estimate of the errors caused by the use of MERRA GPH in our radiative transfer calculations. Better agreement seen at the poles may simply be due to the fact that there are not many measurements at these latitudes and both may be influenced by the same climatology.

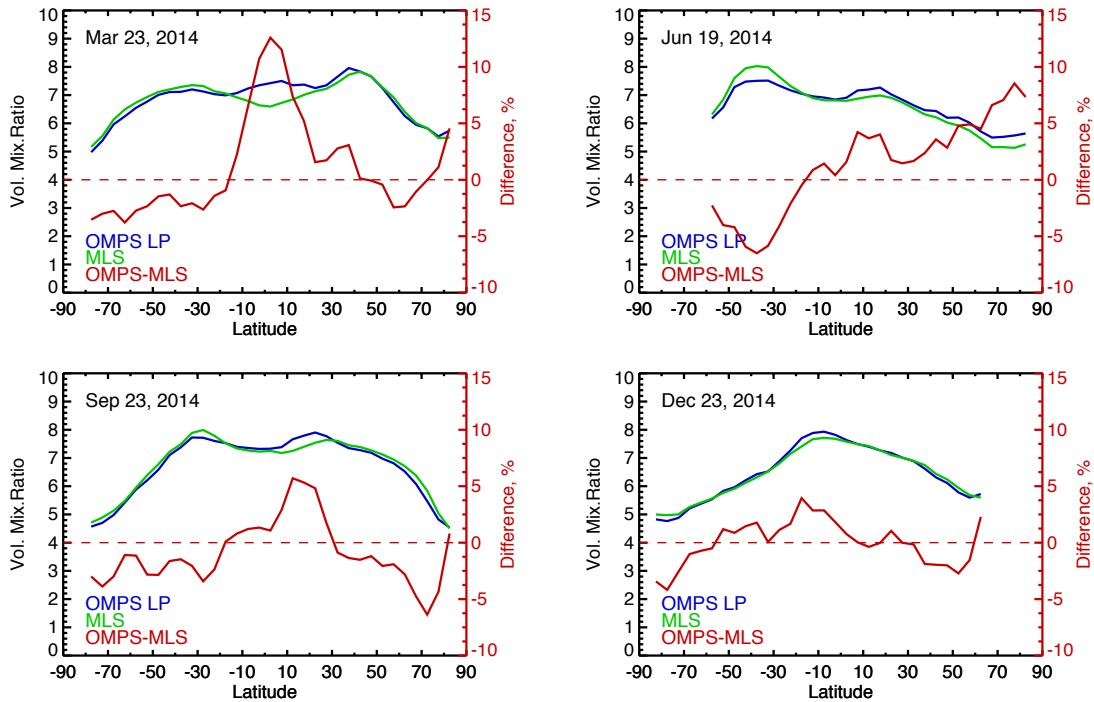


Figure 12: We have estimated the DUR modeling error by comparing 353 nm measured and modeled radiances at 3 hPa. The radiances are modeled using an independent, nearly simultaneous measure of surface reflectivity derived from the OMPS Nadir instrument at 340 nm. The 50x50 km nadir-view measurements are relatively insensitive to DUR effects. The radiance differences (given for the same four cardinal days as in Fig. 10) suggests model or calibration errors of 2-3% on average, plus structure caused by the contributing limb and nadir scene mismatch. If this error were attributed solely to the limb model and only at one altitude, the resulting TH error would be less than +/-200 m. There is no evidence of either a seasonal or a latitude dependence in the comparison, meaning that DUR effects cannot explain the variations seen in Fig. 9.

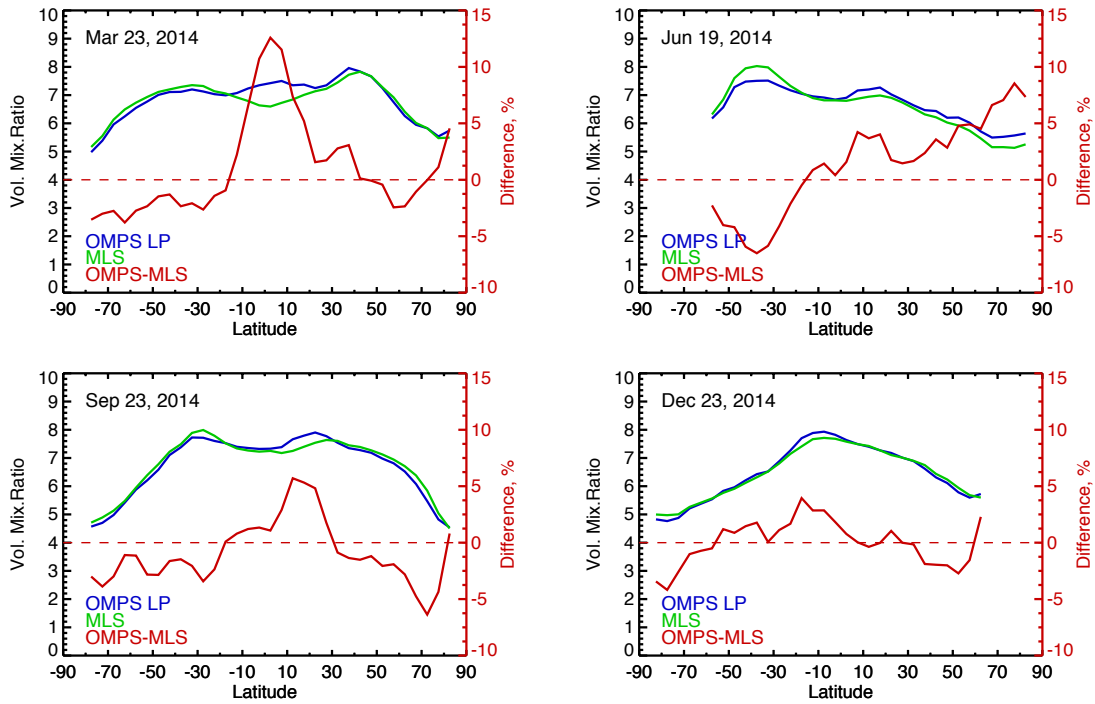


Figure 13: Daily 5 degree zonal means of ozone from MLS (blue), GMAO (green), and the MLS- GMAO differences (red) at 3 hPa GPH for four cardinal days. The differences are generally within 6% which if completely attributed to TH error would be ~200 m.

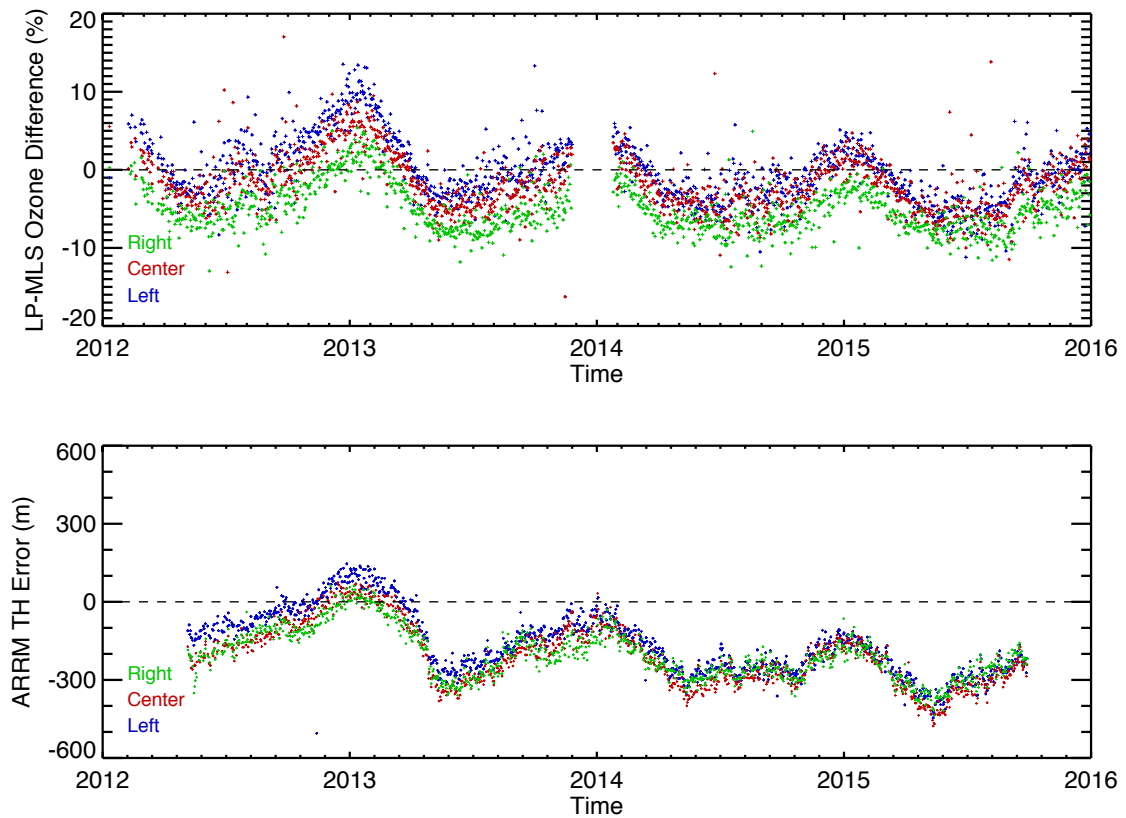


Figure 14: The time series of daily zonal mean ozone differences (%) between OMPS LP and Aura MLS for the 3 slits (top). OMPS LP profiles are corrected with the TH error shown in Table 1. Note the similarity in time-dependent patterns for ozone differences and TH error derived from AARM method (bottom, reprinted from Fig.9). The fact that these two completely independent methods show very similar patterns give us additional confidence in the AARM method.